

Optical properties of $\text{Zn}_{1-x}\text{Mg}_x\text{O}$ nanorods using catalysis-driven molecular beam epitaxy

Y.W. Heo^{a,*}, M. Kaufman^a, K. Pruessner^a, D.P. Norton^{a,*}, F. Ren^b,
M.F. Chisholm^c, P.H. Fleming^c

^a Department of Materials Science and Engineering, University of Florida, P.O. Box 116400,
Rhines Hall, Gainesville, FL 32606, USA

^b Department of Chemical Engineering, University of Florida, Gainesville, FL 32606, USA

^c Oak Ridge National Laboratory, P.O. Box 2008, Oak Ridge, TN 37831, USA

Received 21 October 2002; received in revised form 4 December 2002; accepted 2 January 2003

Abstract

We report on the optical properties of (Zn,Mg)O nanorods grown by catalyst-driven molecular beam epitaxy. The process is site-specific, as single crystal (Zn,Mg)O nanorod growth is realized via nucleation on Ag films or islands that are deposited on a SiO₂-terminated Si substrate surface. Growth occurs within a flux of Zn, Mg, and O₂/O₃ mixture at substrate temperatures of 400–500 °C. With the addition of Mg, the nanorod morphology becomes more uniform relative to the pure ZnO nanomaterials synthesized under similar conditions. The (Zn,Mg)O nanorods are cylindrical, exhibiting diameters of 15–40 nm and lengths in excess of 1 μm. The (Zn,Mg)O nanorods exhibit a strong photoluminescence response, showing a slight shift to shorter wavelengths due to Mg incorporation.

© 2003 Elsevier Ltd. All rights reserved.

Keywords: ZnMgO; Nanorods; Photoluminescence; Molecular beam epitaxy

The optical and electronic properties of nanoscale materials in the form of superlattices (2-D), nanowires (1-D) and nanodots (0-D) is an area of significant interest [1]. One of the most attractive classes of materials for functional nano-devices are semiconductors. The synthesis of semiconducting nanowires and nanorods has been reported using various techniques [2–4]. Nano-device functionality has been demonstrated with these materials in the form of electric field-effect switching [5], single electron transistors [6], biological and chemical sensing [7], and luminescence [8] for 1-D semiconducting structures. Nanostructured semiconducting oxides, such as Ga₂O₃ [9], In₂O₃ [10], and ZnO [11–26], are of interest based on their photonic, electronic, and sensor-related

properties. Of these, zinc oxide is particularly interesting for nano-device applications. ZnO is an n-type, direct bandgap semiconductor with $E_g = 3.35$ eV [27,28]. Electron doping via defects originates from Zn interstitials in the ZnO lattice. The intrinsic defect levels that lead to n-type doping lie approximately 0.05 eV below the conduction band. The room temperature Hall mobility in ZnO single crystals is among the highest for the oxide semiconductors, on the order of 200 cm² V⁻¹ s⁻¹. The bandgap of ZnO can be increased via Mg cation substitution. The exciton binding energy is on the order of 60 meV in ZnO, yielding efficient luminescence at room temperature. As a gas sensor material based on the near-surface modification of charge distribution with certain surface-absorbed species, ZnO nanorods would provide significant enhancement in sensitivity due to high surface-to-volume ratio [29]. ZnO is also piezoelectric, and is used in surface acoustic wave devices [30]. One can envision the exploration of nano-acoustic

* Corresponding authors. Tel.: +1-352-846-1091; fax: +1-352-846-1182 (Y.W. Heo).

E-mail address: ywheo@mse.ufl.edu (Y.W. Heo).

device concepts using ZnO nanorods. As a direct bandgap semiconductor, ZnO nanorods are also attractive as an optical material. Room-temperature ultraviolet lasing via optical pumping has been demonstrated with ZnO nanorods on deposited Au catalyst using a high-temperature vapor transport process [8]. As with any semiconductor, 1-D ZnO nanostructures provide an attractive candidate system for fundamental quantization studies. In semiconductors, quantum effects should be observable for low-dimensional structures with length scales on the order of the exciton Bohr radius [31,32]. For ZnO, with an effective mass of $\sim 0.24 m_e$, the exciton Bohr radius is 17 Å. The formation of 1-D nanostructures for probing low-dimensional effects such as quantization, interface scattering, and ballistic transport should be possible.

The synthesis of ZnO nanowires and nanorods has been demonstrated using vapor-phase transport via a vapor–liquid–solid mechanisms [33,34], gas reactions [35], and oxidation of metal in the pores of anodic alumina membranes [36,37]. However, little activity has been reported on the formation of (Zn,Mg)O alloy nanorods. Recently, we reported on catalyst-driven molecular beam epitaxy (MBE) of ZnO nanorods [38]. The process is site-specific, as single crystal ZnO nanorod growth is realized via nucleation on Ag films or islands that are deposited on a SiO₂-terminated Si substrate surface. Growth occurs at relatively low substrate temperatures, on the order of 300–500 °C. With this approach, nanorod placement can be predefined via location of metal catalyst islands or particles. This, coupled with the relatively low growth temperatures, suggests that ZnO nanorods could be integrated on device platforms for numerous applications, including chemical sensors, nano-optics, scanning probes and nanoelectronics. For optical applications, the ability to modify the bandgap via doping with Mg would be of significant interest.

In this paper, we report on the synthesis and optical properties of (Zn,Mg)O nanorods using the catalysis-driven MBE method. Low temperature MBE conditions are identified such that (Zn,Mg)O nucleation and growth occurs on the deposited metal catalyst. With this approach, site-specific, single crystal (Zn,Mg)O nanorod growth is achieved with nanorod diameters as small as 15 nm.

The growth experiments were performed using a conventional MBE system schematically illustrated in Fig. 1. The background base pressure of the growth chamber was approximately 5×10^{-8} mbar. An ozone/oxygen mixture was used as the oxidizing source. The nitrogen-free plasma discharge ozone generator yielded an O₃/O₂ ratio on the order of 1–3%. No effort was made to separate the molecular oxygen from the ozone. The cation flux was provided by Knudsen effusion cells using high purity (99.9999%) Zn metal and Mg (99.95%)

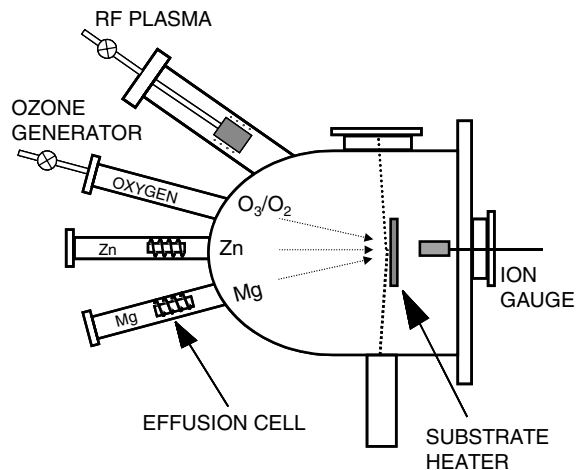


Fig. 1. Schematic of MBE system for nanorod growth.

as the source materials. Cation and O₂/O₃ partial pressure was determined via a nude ionization gauge that was placed at the substrate position prior to growth. The beam pressure of O₃/O₂ mixture was varied between 5×10^{-6} and 5×10^{-4} mbar, controlled by a leak valve between the ozone generator and the chamber. The Zn and Mg pressure was varied between 5×10^{-7} and 4×10^{-6} mbar. The substrates were Si wafers with native SiO₂ layer terminating the surface. No effort was made to remove the native oxide or to terminate the surface with hydrogen.

Site-selective nucleation and growth of Mg-doped ZnO was achieved by coating Si substrates with Ag islands. For nominal Ag film thicknesses of 20–200 Å, discontinuous Ag islands are realized. On these small metal islands, (Zn,Mg)O nanorods were observed to grow. Typical growth times for (Zn,Mg)O on the Ag-coated silicon was 2 h with growth temperatures ranging from $T_g = 300$ –500 °C. After growth, the samples were evaluated by scanning electron microscopy (SEM), transmission electron microscopy (TEM), and photoluminescence.

Fig. 2 shows a SEM image of ZnO nanorods grown at two different temperatures on a Si wafer that was coated with a nominally 10 nm thick layer of Ag. The Ag was deposited using e-beam evaporation. The images are for ZnO nanorods grown with a Zn pressure of 2×10^{-6} Torr and an oxygen/ozone pressure of 5×10^{-4} Torr. Under these conditions, ZnO deposition was observed only on the Ag with no growth on regions of the SiO₂-terminated Si surface that was devoid of Ag. Fig. 2(a) shows a cross-section SEM image of ZnO nanorods and whiskers grown at 400 °C. A dense entangled collection of ZnO nanorods is observed to grow from the surface. Both cylindrical nanorods and faceted whiskers can be observed in the forest of ZnO nanostructures

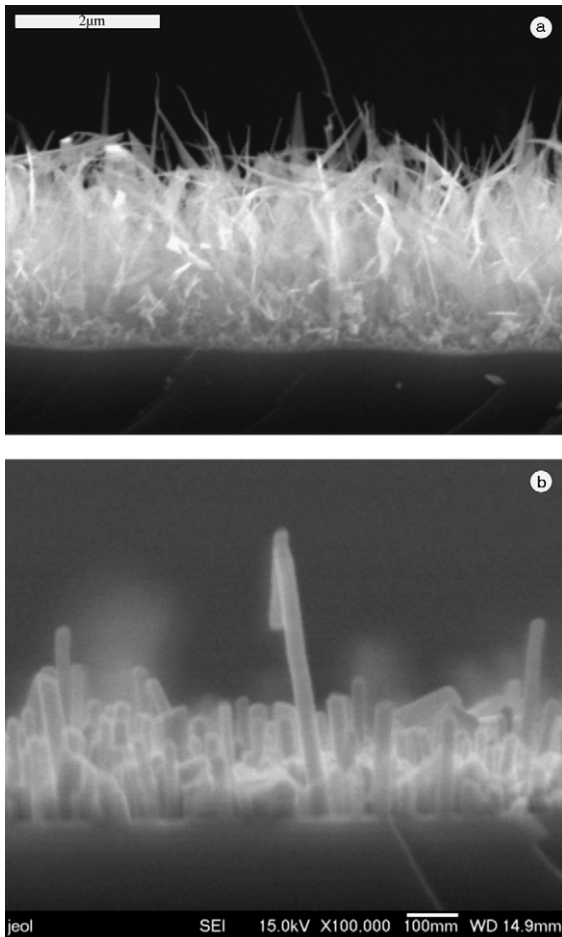


Fig. 2. SEM images of ZnO nanorods nucleated on Ag-coated Si/SiO₂ substrate at (a) 400 °C and (b) 500 °C.

grown at 400 °C. Fig. 2(b) shows the SEM micrograph of ZnO nanorods grown at 500 °C. In this case, only nanorods are observed. In many cases, the length of ZnO nanorods is in excess of 2 μm. Note also that multiple nanorods are observed to nucleate from the relatively large Ag islands. The diameter of the nanorods is not determined by the initial radius of the Ag islands.

The growth of Mg-doped ZnO nanorods was investigated using the same conditions and Ag catalysts as was used before. The high vapor pressures of both Zn and Mg suggest that (Zn,Mg)O nanorod growth should be possible under similar conditions. Fig. 3 shows a FE-SEM image of the (Zn,Mg)O nanorods grown in a Zn pressure of 2×10^{-6} mbar, a Mg pressure of 5×10^{-7} mbar, and an O₂/O₃ pressure of 5×10^{-4} mbar. The nanorods were deposited on a Ag-coated Si wafer with a nominal Ag thickness of 2 nm. The growth temperature was 400 °C. Note that the morphology of the nanorods changes with the addition of Mg. First, only rods are

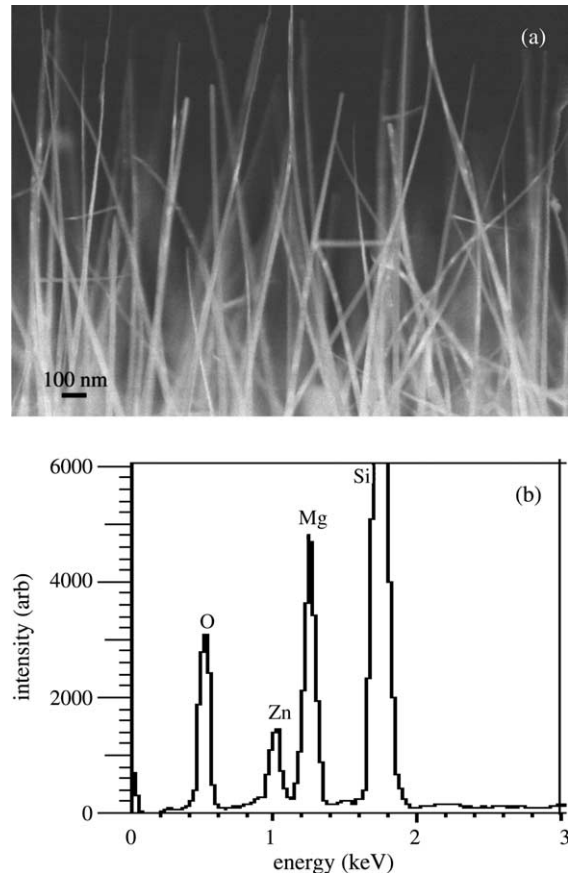


Fig. 3. SEM image of (Zn,Mg)O nanorods grown by catalyst-assisted MBE. Also shown (b) is the energy-dispersive spectrometry data confirming the presence of Mg and Zn in the nanorods.

observed with no whiskers. Second, the distribution of rod diameters becomes more narrow with the addition of Mg flux. Energy-dispersive spectrometry was used to confirm the presence of Mg in the nanorod composition. A Mg peak is clearly present in the figure. From the high-resolution image, the nanorod cross-section appears to be cylindrical. The thickness of the nanorods shown in Fig. 3 is on the order of 30 nm.

In addition to SEM, the (Zn,Mg)O nanorods were examined using TEM. Fig. 4 shows a TEM image of an individual ZnO nanorod. The nanorod shown in Fig. 4 was not carbon-coated. A typical rod thickness is 10 nm. The lattice image for the nanorod specimen indicates that the rod is crystalline with the wurtzite crystal structure. The c axis is oriented along the long axis of the rod. Also evident in the image is a small particle embedded at the tip of the rod. This is similar to what is observed for other nanorod synthesis that is driven by a catalytic reaction, where catalyst particles become suspended on the nanorod tip [39,40].

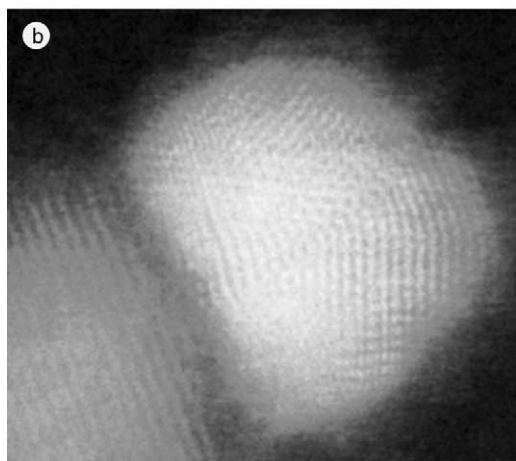
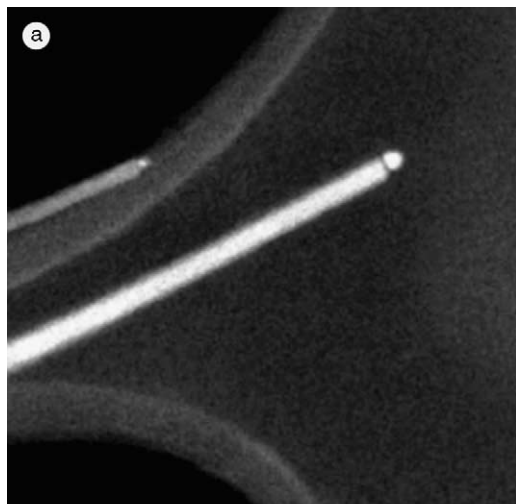


Fig. 4. Scanning transmission electron microscope image of a single crystal (Zn,Mg)O nanorod.

The optical properties of the nanorods were examined using photoluminescence. A He–Cd (325 nm) laser was used as the excitation source. The room-temperature luminescence for a ZnO nanorod specimen is shown in Fig. 5, revealing a robust near band-edge emission peak located at 3.3 eV. This is consistent with luminescence reported for near band edge emission in epitaxial films [41,42] and larger diameter ZnO nanorods [43]. The figure shows the photoluminescence spectrum for rods grown at 400 °C and 500 °C. Clearly the luminescence is higher for the rods grown at 500 °C, reflecting superior crystallinity. Note also that the broadband emission due to defect levels also differs. A broad, but weak, green emission peak is observed at ~2.8 eV for rods grown at 400 °C. This is typically associated with trap-state emission attributed to singly ionized oxygen vacancies in ZnO [44]. The emission is the result of the radiative recombination of photogenerated holes with

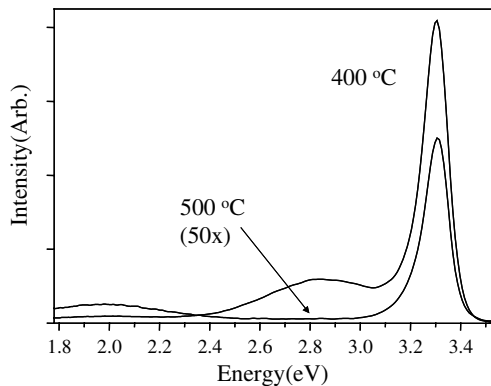


Fig. 5. Photoluminescence spectra for ZnO nanorods grown at 400 and 500 °C.

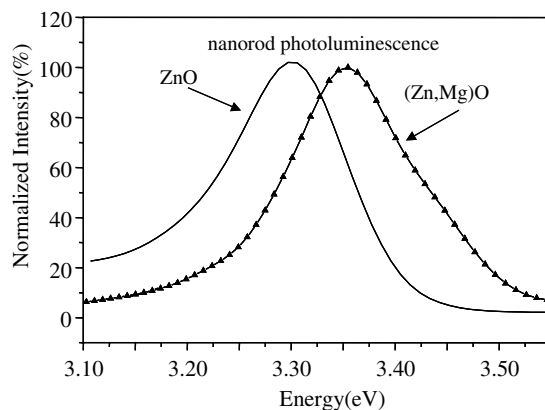


Fig. 6. Comparison of band-edge photoluminescence for ZnO and (Zn,Mg)O nanorods.

electrons occupying the oxygen vacancy. Similar results have been observed for ZnO nanorods formed via vapor transport. However, the nanorods grown at 500° C exhibit a broad emission center at ~2.0 eV. The photoluminescence spectra for the (Zn,Mg)O nanorod samples is shown in Fig. 6. A shift in the photoluminescence peak location is observed, although it is much less than what would be predicted based on the EDS measure of Mg content, as well as has been seen in the luminescence properties of (Zn,Mg)O epitaxial films. Current efforts are exploring the luminescent properties of the Mg-doped ZnO nanorod materials.

Acknowledgement

This work was partially supported by the Army Research Office through grant DAAD19-01-1-0603.

References

- [1] Timp G, editor. Nanotechnology. New York: Springer-Verlag; 1998.
- [2] Wu Y, Yang P. Chem Mater 2000;12:605.
- [3] Morales AM, Lieber CM. Science 1998;279:208.
- [4] Shi WS, Zheng YF, Wang N, Lee CS, Lee ST. J Vac Sci Technol B 2001;19:1115.
- [5] Kim GT, Muster J, Krstic V, Park JG, Park YW, Roth S, et al. Appl Phys Lett 2000;76:1875.
- [6] Stone NJ, Ahmed H. Appl Phys Lett 1998;73:2134.
- [7] Cui Y, Wei Q, Park H, Lieber CM. Science 2001;293:1289.
- [8] Huang MH, Mao S, Feick H, Yan H, Wu Y, Kind H, et al. Science 2001;292:1897.
- [9] Zhang HZ, Kong YC, Wang YZ, Du X, Bai ZG, Wang JJ, et al. Solid State Commun 1999;109:677.
- [10] Zheng MJ, Zhang LD, Li GH, Zhang XY, Wang XF. Appl Phys Lett 2001;79:839.
- [11] Kovtyukhova NI, Martin BR, Mbindyo JKN, Smith PA, Razavi B, Mayer TS, et al. J Phys Chem B 2001;105:8762.
- [12] Pan ZW, Dai ZR, Wang ZL. Science 2001;291:1947.
- [13] Sun XM, Chen X, Deng ZX, Li YD. Mater Chem Phys 2003;78:99.
- [14] Park WI, Jung SW, Yi G-C, Oh SH, Park CG, Kim M. Jpn J Appl Phys 2002;41:L1206.
- [15] Mcguire K, Pan ZW, Wang ZL, Milkie D, Menendez J, Rao AM. J Nanosci Nanotechnol 2002;2:499.
- [16] Wu J-J, Liu S-C. J Phys Chem B 2002;106:9546.
- [17] Kim H, Sigmund W. Appl Phys Lett 2002;81:2085.
- [18] Park WI, Kim DH, Jung S-W, Yi G-C. Appl Phys Lett 2002;80:4232.
- [19] Dai Y, Zhang Y, Li QK, Nan CW. Chem Phys Lett 2002;358:83.
- [20] Dloczik L, Engelhardt R, Ernst K, Lux-Steiner MC, Konenkamp R. Sens Actuators B (Chem) B 2002;84:33.
- [21] Wang ZL, Pan Z. Int J Nanosci 2002;1:41.
- [22] Vayssieres L, Guo J, Nordgren J. Nanoparticulate materials. In: Materials Research Society Symposium Proceedings, vol. 704, 2002. p. 335–41.
- [23] Xu C, Xu G, Liu Y, Wang G. Solid State Commun 2002;122:175.
- [24] Li JY, Chen XL, Li H, He M, Qiao ZY. J Cryst Growth 2001;233:5.
- [25] Li JY, Chen XL, Wei ZF, Qiao ZY. Chin Phys Lett 2001;18:1527.
- [26] Guo L, Cheng JX, Li X-Y, Yan YJ, Yang SH, Yang CL, et al. Mater Sci Eng C, Biomimetic Supramol Syst 2001; C16:123.
- [27] Look DC, Hemsley JW, Sizelove JR. Phys Rev Lett 1999; 82:2552.
- [28] Hutson AR. Phys Rev 1957;108:222.
- [29] Kang WP, Kim CK. Sens Actuators B 1993;13–14:682.
- [30] Van de Pol FCM. Ceram Bull 1990;69:1959.
- [31] Wong EM, Searson PC. Appl Phys Lett 1999;74:2939.
- [32] Ohtomo A, Kawasaki M, Ohkubo I, Koinuma H, Yasuda T, Segawa Y. Appl Phys Lett 1999;75:980.
- [33] Kong YC, Yu DP, Zhang B, Fang W, Feng SQ. Appl Phys Lett 2001;78:407.
- [34] Huang MH, Wu Y, Feick H, Tran N, Weber E, Yang P. Adv Mater 2001;13:113.
- [35] Tang CC, Fan SS, de la Chapelle ML, Li P. Chem Phys Lett 2001;333:12.
- [36] Li Y, Meng GW, Zhang LD, Phillip F. Appl Phys Lett 2000;76:2011.
- [37] Hulteen JC, Martin CR. J Mater Chem 1997;7:1075.
- [38] Heo YW, Varadarajan V, Kaufman M, Kim K, Ren F, Fleming PH, et al. Appl Phys Lett 2002;81:3046.
- [39] Lee ST, Wang N, Lee CS. Mater Sci Eng A 2000;286:16.
- [40] Liang CH, Meng GW, Wang GZ, Wang YW, Zhang LD, Zhang SY. Appl Phys Lett 2001;78:3202.
- [41] Sakurai K, Iwata D, Fujita S, Fujita S. Jpn J Appl Phys 1999;38:2606.
- [42] Johnson MAL, Fujita S, Rowland Jr WH, Hughes WC, Cook Jr JW, Schetzina JF. J Electron Mater 1996;25:855.
- [43] Kong YC, Yu DP, Zhang B, Fang W, Feng SQ. Appl Phys Lett 2001;78:407.
- [44] Vanheusden K, Warren WL, Seager CH, Tallant DK, Voigt JA, Gnade BE. J Appl Phys 1996;79:7983.